Available online at www.sciencedirect.com
SCIENCE DIRECT
Journal of Sound and Vibration 294 (2006) 298–313
JOURNAL OF SOUND AND VIBRATION
www.elsevier.com/locate/jsvi

# Deployment of a multi-link flexible structure

Kyung-Su Na, Ji-Hwan Kim*

*School of Mechanical and Aerospace Engineering, Seoul National University, San 56-1, Shinrim-Dong, Kwanak-Ku, Seoul 151-742, Republic of Korea*

Received 29 October 2004; received in revised form 3 November 2005; accepted 19 November 2005
Available online 30 January 2006

**Abstract**

Deployment of a multi-link beam structure undergoing locking is analyzed in the Timoshenko beam theory. In the modeling of the system, dynamic forces are assumed to be torques and restoring forces due to the torsion spring at each joint. Hamilton's principle is used to determine the equations of motion and the finite element method is adopted to analyze the system. Newmark time integration and Newton–Raphson iteration methods are used to solve for the non-linear equations of motion at each time step. The locking at the joints of the multi-link flexible structure is analyzed by the momentum balance method. Numerical results are compared with the previous experimental data. The angles and angular velocities of each joint, tip displacement, and velocity of each link are investigated to study the motions of the links at each time step. To analyze the effect of thickness on the motion of the link, the angle and the tip displacement of each link are compared according to the various slenderness ratios. Additionally, in order to investigate the effect of shear, the tip displacements of a Timoshenko beam are compared with those of an Euler–Bernoulli beam.


## 1. Introduction

Deployment of structures, such as the solar arrays, antennas and robot arms, etc. has been studied actively. In modern applications, the weights of these structures have to be minimized, and hence various advanced materials have been tried. As a result of weight minimization, these structures will have relatively low structural rigidity. Researches have been tried to improve the accuracy in the operation of flexible structures.

Meirovitch and Chen [1] analyzed a two-link beam structure using Euler–Bernoulli beam theory. This analysis supported their study of a flexible space robot whose mission is to ferry some payload in space, and dock smoothly with an orbiting target. Yigit [2] studied the impact response of beam structures. The first link was modeled as a rigid-body and the second link was analyzed under the Euler–Bernoulli beam theory. Further, a spring-dashpot model was used for impact analysis. Yu and Elbestawi [3] studied the dynamic characteristics of a two-link planar flexible manipulator with large joint angular motions. The links and joints of the manipulator were assumed to be very flexible and effects by internal structural damping, dry friction at the joints, and backlash between driving gears were additionally considered. The dynamic equations of this system, modeled as Euler–Bernoulli beams, were analyzed and verified with the experimental results. Ge et al.

*Corresponding author. Tel.: +82 2 880 7383; fax: +82 2 887 2662.
*E-mail address:* jwhkim@snu.ac.kr (J.-H. Kim).

0022-460X/$ - see front matter © 2006 Elsevier Ltd. All rights reserved.
doi:10.1016/j.jsv.2005.11.018

[4] studied the non-model-based position control of a planar robot, which was modeled by the Euler–Bernoulli beam theory. Numerical simulations were performed on a two-link flexible robot. Nagaraj and Nataraju [5] proposed a mathematical model for a flexible system that undergoes locking during motion. They used Euler–Bernoulli beam theory and the momentum balance method to model the locking at each joint. In addition, experiments for the two flexible aluminum links with a revolute joint at the end of each link were performed. Fung and Chang [6] derived the equations of motion for a nonlinear, constrained flexible manipulator with a tip mass by using Hamilton's principle. Four dynamic models, based on Timoshenko, Euler–Bernoulli, simple flexure and rigid-body beam theory, were used to describe flexible two-link or single manipulators. Milford and Asokanthan [7] analyzed the eigenfrequencies of a system composed of Euler–Bernoulli beams. They derived the eigenfrequencies of a flexible robot manipulator with a locked elbow and compared the numerical results with the experimental data. Chen [8] studied a linear dynamic model for multi-link planar flexible manipulators with an arbitrary number of flexible links. Elastic deformation of each link was modeled by the assumed-mode method, and the flexible links were treated as Euler–Bernoulli beams. To verify the proposed method, two planar manipulators were simulated, and results were presented. Hariharesan and Barhorst [9] studied the modeling, simulation and experimental verification of contact/impact dynamics of a flexible multi-body system by using the Euler–Bernoulli beam theory. In this work, the contact/impact of a flexible multi-body system undergoing pre-contact free motion, and the contact/impact and post-impact under constraint motion were modeled. The model was experimentally validated using a planar flexible manipulator that completed a full motion regime. Escalona et al. [10] analyzed some aspects of the application of the generalized impulse-momentum balance method to flexible multi-body systems. Farid and Lukasiewicz [11] studied the dynamic modeling of spatial manipulators based on Euler–Bernoulli beam theory. The dynamic model was free from the assumption of a nominal motion. In addition, it considered the coupling effects between the rigid body motion and the elastic deformations of the links as well as the interaction between flexible links and actuated joint. Naganathan and Soni [12] studied the effects of coupling on the kinematics and flexibility in manipulators. Governing equations of motion were derived including those representing the effects of rotary inertia, shear deformation and gross nonlinear motion of each link. The complete dynamic model was further integrated with a simplistic actuator-servo model. Iura and Atluri [13] presented an efficient formulation for the dynamics of the Timoshenko beam with finite rotations. They assumed that the beam was a rotating frame showing small strain to obtain the strain energy of the system. Cheong et al. [14] investigated the accessibility and identifiability of horizontal vibration in 3-D two-link flexible robots with system mode approach. They adopted system mode vibration analysis for interpreting the equations of motion, depending on configurations, in relation to rigid-flexible coupled dynamics. Theodore and Ghosal [15] discussed the robustness and stability issues in a model-based trajectory tracking controller which uses a finite element model of the multi-link flexible manipulators. Dynamic equations of motion were obtained by using Lagrangian formulation. A robust controller design based on the second method of Lyapunov, using simple quantitative bounds on the model uncertainties, was illustrated.

In the previous works, shear deformation effect was not considered in analysis of a flexible multi-link beam undergoing locking. The effect of shear deformation on the deployment of relatively thick links may be significant. Likewise, in this study we investigated the deployment of a multi-link Timoshenko beam undergoing locking during the motion. Each link has a lumped mass at the tip, and the dynamic forces for deployment are assumed to be torques and restoring forces, generated by the torsion spring at each joint. Joint angle, velocity and tip displacement of each link is compared with those for a rigid-body. The comparison of the results of a two-link Timoshenko beam analysis to the previous experimental data is discussed in detail. In order to analyze the effect of thickness, the angle and the tip displacement of each link are compared according to the various slenderness ratios. In addition, to investigate the effect of shear, the tip displacements of a Timoshenko beam are compared with those of an Euler–Bernoulli beam.

## 2. Formulation

### 2.1. System modeling

Fig. 1 shows the motion of a multi-link beam structure, and $n$ denotes the total number of links. The rotational velocity is fastest at the $n$th link and lowest at first link. The farther away the link is from a fixed

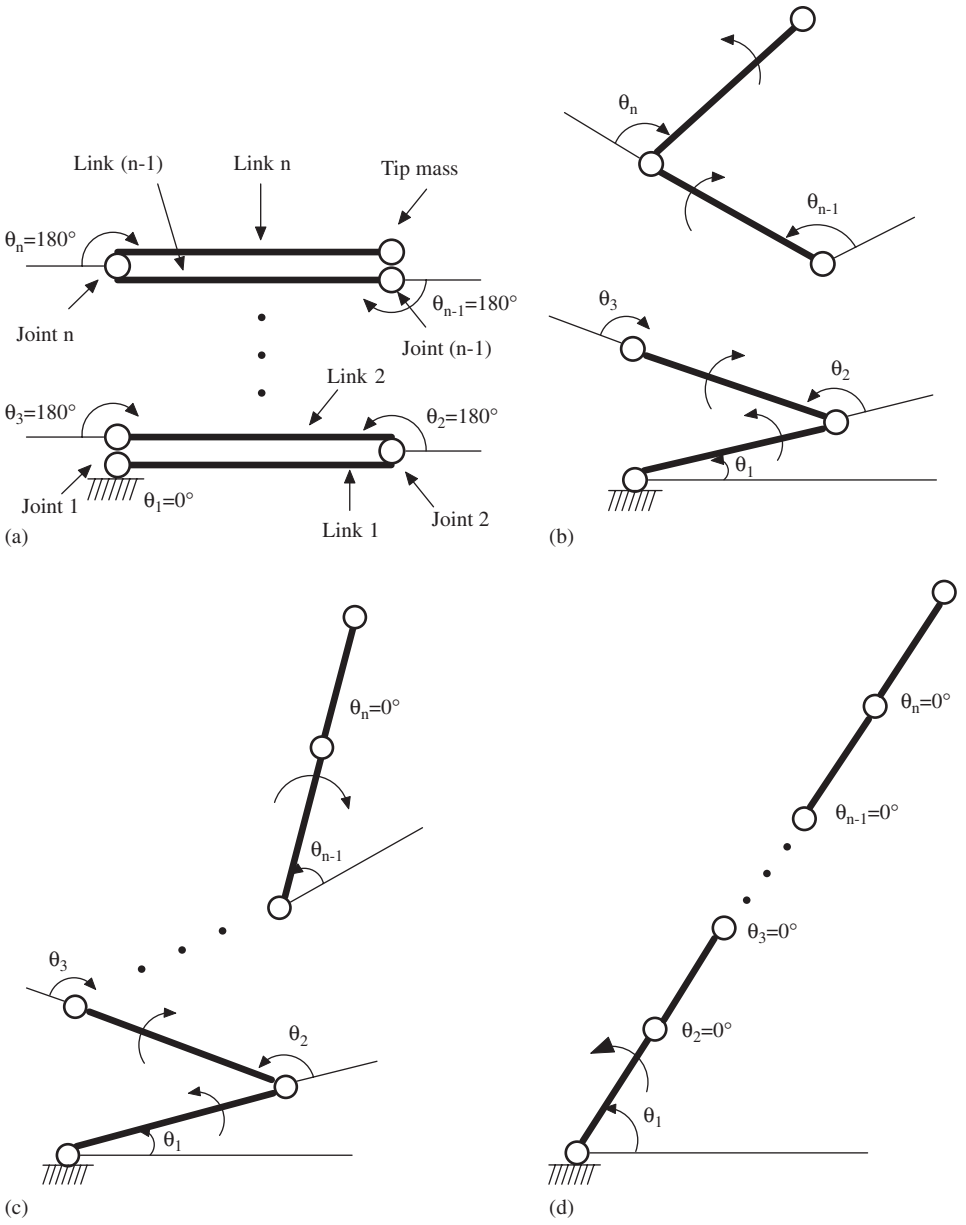


Fig. 1. Diagram of the motion for the multi-link Timoshenko beam: (a) Initial state; (b) first motion; (c) first stage of locking; (d) ($n-1$)th stage of locking.

origin (joint 1), the faster its rotational velocity becomes. Thus the locking occurs successively during motion, from the last two links to the first two links. The initial state of the $n$-link Timoshenko beam is shown in Fig. 1(a). All links are folded at known initial angles, and each joint is characterized by the behavior of a torsion spring. Fig. 1(b) illustrates the first motion of the links. Each link, when released from its initial configuration, rotates about each joint. This first motion is denoted as the first phase. The first stage of locking occurs when the angle between the ($n-1$)th and the $n$th link is zero, as shown in Fig. 1(c). After locking, the torque acting at link $n$ disappears. In addition, the $n$th joint loses its rotational degree of freedom and then both the ($n-1$)th and $n$th link rotate about the ($n-1$)th joint, like a single flexible link. The motion after first locking is denoted as the second phase. Likewise, after the ($n-1$)th locking, the second joint loses its rotational degree of freedom and all links rotate about the first joint, like a single flexible link, as represented in Fig. 1(d).

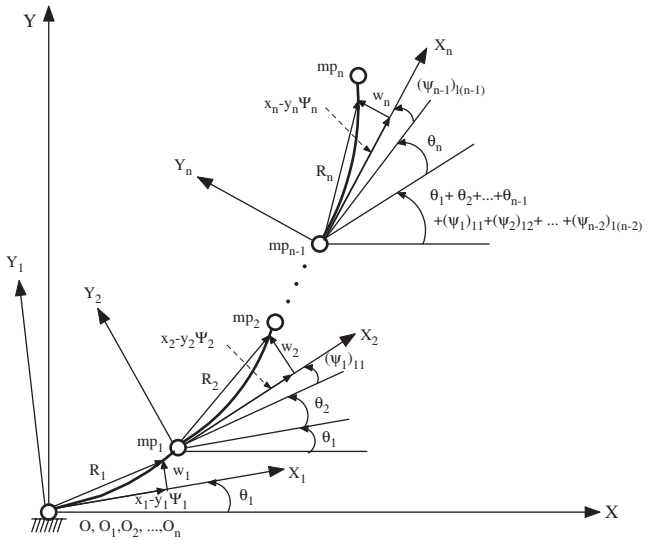


Fig. 2. Model of the multi-link flexible system.

The motion after $(n-1)$th locking is denoted as the $n$th phase. This assumption of mechanism can be achieved by tuning the springs, inertia of links and preloaded torques.

In this study, the system is assumed to operate in the horizontal plane. Each link is considered to have a constant cross-sectional area and isotropic material properties.

Fig. 2 shows the multi-link flexible system in its original and deformed configuration. Each link is modeled based on Timoshenko beam theory. In this, $OXY$ indicates the fixed original coordinate system and $O_iX_iY_i$ is the moving local coordinate system of link $i$. The relative joint angle of each link is denoted by $\theta_i$. The bending deflection and the rotation angle of the normal to the neutral axis, with respect to its local coordinate, are given as $w_i$ and $\psi_i$, respectively. The local coordinate, length and tip mass of link $i$ are denoted by $(x_i, y_i)$, $l_i$ and $m_i$, respectively.

The vector $\mathbf{r}_{oi}$ indicates the position of any point on link $i$ from the origin of the fixed coordinate system of the link

$$\mathbf{r}_{oi} = \mathbf{r}_i + \mathbf{T}_i\mathbf{R}_i, \tag{1}$$

where the vector $\mathbf{r}_i$ represents the position of the origin for the local coordinate of link $i$ and the vector $\mathbf{R}_i$ presents the elastic deformation of link $i$ with respect to the local coordinate system. In addition, $\mathbf{T}_i$ is the transformation matrix that relates the local coordinate system to the fixed one:

$$\mathbf{R}_i = \begin{Bmatrix} x_i + u_i \\ y_i + w_i \end{Bmatrix}, \quad \mathbf{T}_i = \begin{bmatrix} \cos(\beta_i) & -\sin(\beta_i) \\ \sin(\beta_i) & \cos(\beta_i) \end{bmatrix}.$$

In these equations, $u_i(x_i, t)$ is the displacement in the $x$ directions of link $i$, and $\beta_i$ is the rotation of joint $i$ with respect to the original coordinate system

$$u_i(x_i, t) = -y_i\psi_i(x_i, t), \quad \beta_i = \begin{cases} \theta_i & \text{for } i = 1 \\ \sum_{j=1}^{i} \theta_j + \sum_{j=1}^{i-1} (\psi_j)_{l_j} & \text{for } i = 2, 3, 4, \ldots, n \end{cases}$$

where $(\psi_j)_{l_j}$ is the rotation angle of the normal to the neutral axis on the tip of link $j$, and $i$ is the total number of joints in the system

The position vector $\mathbf{r}_{omi}$ of the tip mass of link $i$ is given by

$$\mathbf{r}_{omi} = \mathbf{r}_i + \mathbf{T}_i\mathbf{R}_{l_i}, \tag{2}$$

where the vector $\mathbf{R}_{l_i}$, presents the elastic deformation of tip mass on link $i$ with respect to the local coordinate system

$$\mathbf{R}_{l_i} = \{l_i \quad (w_i)_{l_i}\}^{\mathrm{T}},$$

where $(w_i)_{l_i}$ is the bending deflection of tip mass on link $i$ with respect to the local coordinate system.

The total kinetic energy of this system is comprised of the motion of the links, tip masses and joints. From Eq. (1), the kinetic energy $T_{ki}$ of link $i$ is given by

$$T_{ki} = \frac{1}{2}\int_{v_i} \rho_i \left[\frac{\mathrm{d}\mathbf{r}_{oi}}{\mathrm{d}t}\right]^{\mathrm{T}} \left[\frac{\mathrm{d}\mathbf{r}_{oi}}{\mathrm{d}t}\right] \mathrm{d}v_i, \tag{3}$$

where $\rho_i$ is the mass density per unit volume of link $i$.

From Eq. (2), the kinetic energy $T_{mi}$ of each tip mass located at the tip of link $i$ is given by

$$T_{mi} = \frac{1}{2} m_i \left[\frac{\mathrm{d}\mathbf{r}_{omi}}{\mathrm{d}t}\right]^{\mathrm{T}} \left[\frac{\mathrm{d}\mathbf{r}_{omi}}{\mathrm{d}t}\right]. \tag{4}$$

The kinetic energy of joint $i$ is given by

$$T_{li} = \tfrac{1}{2} J_i \dot{\beta}_i^{\mathrm{T}} \dot{\beta}_i, \tag{5}$$

where $J_i$ is the joint rotary inertia, and $\dot{\beta}_i$ is the angular velocity of joint $i$.

Therefore, the total kinetic energy $T$ of the system can be expressed as

$$T = \sum_{i=1}^{n} (T_{ki} + T_{mi} + T_{li}), \tag{6}$$

where $n$ is the total number of links in the system.

The total potential energy of the multi-link beam system is divided into two parts. The strain energy $V_{li}$ due to the elastic deformations of links and the potential energy $V_s$ due to the torsion springs at the joints.

First, the strain energy $V_{li}$ of link $i$ is given by

$$V_{li} = \frac{1}{2}\int_0^{l_i} E_i I_i \left(\frac{\mathrm{d}\psi_i}{\mathrm{d}x_i}\right)^2 + k_i G_i A_i \left(\frac{\mathrm{d}w_i}{\mathrm{d}x_i} - \psi_i\right)^2 \mathrm{d}x_i, \tag{7}$$

where $E_i$, $I_i$, $k_i$, $G_i$ and $A_i$ denote Young's modulus, moment of inertia, shear deformation coefficient, shear modulus of elasticity and cross-sectional area of link $i$, respectively.

Second, the potential energy $V_s$ due to the torsion spring at joint $i$ is given by

$$V_s = \frac{1}{2}\sum_{i=1}^{n_j} k_{si}(\theta_{0i} - \theta_i)^2, \tag{8}$$

where $k_{si}$ is the torsion spring stiffness and $\theta_{0i}$ is the pre-rotation angle of the joint $i$.

Therefore, total potential energy $V$ of the system can be expressed as

$$V = V_s + \sum_{i=1}^{n} V_{li}. \tag{9}$$

The virtual work of the system is expressed as

$$\delta W = \sum_{i=1}^{n_j} \tau_i \delta\theta_i, \tag{10}$$

where $\tau_i$ is friction torque due to the spring force exerted by the rocker arm at joint $i$ [2,3,5] and $n_j$ indicates the total number of joints in the system.

Each joint of link $i$ has only a rotational degree of freedom, thus the boundary conditions at the link $i$ are as follows:

$$w_{0i} = 0 \quad \text{and} \quad \psi_{0i} = 0 \quad \text{at } x_i = 0. \tag{11}$$

Equations of motion can be derived by using Hamilton's principle as follows:

$$\int_{t_1}^{t_2} (\delta T - \delta V - \delta W)\, \mathrm{d}t = 0. \tag{12}$$

By using the finite element method, the following discrete equation of motion is obtained:

$$[\mathbf{M}(\mathbf{q})]\{\ddot{\mathbf{q}}\} + [\mathbf{C}(\mathbf{q}, \dot{\mathbf{q}})]\{\dot{\mathbf{q}}\} + [\mathbf{K}]\{\mathbf{q}\} = \{\mathbf{W}\}, \tag{13}$$

where $\{\mathbf{q}\}$ is $\{w_1 \;\; w_2 \ldots w_{n_d} \;\; \psi_1 \;\; \psi_2 \ldots \psi_{n_d} \;\; \theta_1 \;\; \theta_2 \ldots \theta_{n_j}\}^{\mathrm{T}}$, and $n_d$ is the total number of nodes and $n_j$ is the total number of joints in the system. $[\mathbf{M}(\mathbf{q})]$ is the mass matrix, containing the rigid body terms, coupling of the rigid body and flexible variables, and the terms of only the flexible variables. $[\mathbf{C}(\mathbf{q}, \dot{\mathbf{q}})]$ is the matrix composed of Coriolis and centripetal terms, $[\mathbf{K}]$ is the stiffness matrix containing the stiffness coefficients of the torsion spring and the links, and $\{\mathbf{W}\}$ is the matrix containing the terms for torques.

Newmark time integration method [16] and Newton–Raphson iteration methods are applied to solve the nonlinear equation of motion at each time step.

### 2.2. Mathematical model for locking

The first stage of locking occurs, when the angle between link $(n-1)$ and link $n$ is zero. In the same way, the $i$th stage of locking occurs, when the angle between link $(n-i)$ and link $(n-i+1)$ is zero $(i = 1, 2, 3, \ldots, n-1)$. Based on the impulse momentum law, post-locking $\{\dot{\mathbf{q}}\}$ is obtained by using the momentum balance method [5,10]. This method assumes instantaneous impact and continuous system configuration during impact. Additionally the velocities are assumed to be bounded during impact. From this method, following equations can be obtained:

$$\{\mathbf{q}_{m+1}\} = \{\mathbf{q}_m\}, \tag{14}$$

where the subscript $m+1$ indicates $\{\mathbf{q}\}$ just after locking and $m$ indicates $\{\mathbf{q}\}$ just before locking.

When the first locking occurs, the matrix $\{\mathbf{W}\}$ from Eq. (13) is expressed as

$$\{\mathbf{W}\} = \{\mathbf{W}_a\} + \{\mathbf{W}_p\}, \quad \{\mathbf{W}_p\} = \mathbf{F}_p\, \mathrm{d}s/\mathrm{d}\mathbf{q}, \tag{15}$$

where $\{\mathbf{W}_a\}$ is the set of generalized external forces and $\{\mathbf{W}_p\}$, $\mathbf{F}_p$ and $s$ indicate the set of impulse forces due to impact, the impact force and the Cartesian coordinate, respectively [5,10,17].

Integrating over the impact period $t$, the equation of motion (13) yields,

$$\int_t^{t+\Delta t} [\mathbf{M}(\mathbf{q})]\{\ddot{\mathbf{q}}\}\, \mathrm{d}t + \int_t^{t+\Delta t} [\mathbf{C}(\mathbf{q}, \dot{\mathbf{q}})]\{\dot{\mathbf{q}}\}\, \mathrm{d}t + \int_t^{t+\Delta t} [\mathbf{K}]\{\mathbf{q}\}\, \mathrm{d}t = \int_t^{t+\Delta t} \{\mathbf{W}\}\, \mathrm{d}t. \tag{16}$$

From the assumptions of the momentum balance method, as the contact duration approaches zero, the integral of the two terms $\{\mathbf{W}_a\}$ and $[\mathbf{C}(\mathbf{q}, \dot{\mathbf{q}})]$ approaches zero, as well. In addition, other matrices can be expressed as the following:

$$\lim_{\Delta t \to 0} \int_t^{t+\Delta t} [\mathbf{M}(\mathbf{q})]\{\ddot{\mathbf{q}}\}\, \mathrm{d}t = [\mathbf{M}(\mathbf{q})]\Delta\{\dot{\mathbf{q}}\}, \quad \lim_{\Delta t \to 0} \int_t^{t+\Delta t} \{\mathbf{W}\}\, \mathrm{d}t = \frac{\mathrm{d}s}{\mathrm{d}\mathbf{q}} \lim_{\Delta t \to 0} \int_t^{t+\Delta t} \{\mathbf{F}_p\}\, \mathrm{d}t. \tag{17}$$

From Eqs. (16) and (17), the following equation is derived:

$$[\mathbf{M}(\mathbf{q})]\Delta\{\dot{\mathbf{q}}\} = \frac{\mathrm{d}s}{\mathrm{d}\mathbf{q}} \lim_{\Delta t \to 0} \int_t^{t+\Delta t} \{\mathbf{F}_p\}\, \mathrm{d}t. \tag{18}$$

Hence, $\{\dot{\mathbf{q}}\}$ after first locking can be written as

$$\{\dot{\mathbf{q}}_{m+1}\} = \{\dot{\mathbf{q}}_m\} + \Delta\{\dot{\mathbf{q}}\}. \tag{19}$$

$\{\dot{\mathbf{q}}\}$ after $i$th locking can be obtained in the same manner.

### 2.3. Equations of motion after locking

For the $n$-link flexible system, when the angle between link $(n-1)$ and link $n$ is zero, the first stage of locking has occurred, as shown in Fig. 1(c). After the first locking, the torque acting at link $n$ disappears. In addition, $n$th joint loses its rotational degree of freedom and link $(n-1)$, and $n$ rotate about the $(n-1)$th joint, like a single flexible link (second phase). Thus the two links of length $l_{n-1}$ and $l_n$ form a single link of length $(l_{n-1}+l_n)$ and the $n$-link flexible system turns into a $(n-1)$-link flexible system. The initial coordinates and velocities of this system are obtained by the momentum balance method. The equation of the $(n-1)$-link flexible system is derived in the similar manner as that of the multi-link flexible system described before.

The equation of motion for a $(n-1)$-link flexible link can be written as

$$[\mathbf{M}_2(\mathbf{q}_2)]\{\ddot{\mathbf{q}}_2\}+[\mathbf{C}_2(\mathbf{q}_2,\dot{\mathbf{q}}_2)]\{\dot{\mathbf{q}}_2\}+[\mathbf{K}_2]\{\mathbf{q}_2\}=\{\mathbf{W}_2\}, \tag{20}$$

where $\{\mathbf{q}_2\}$ is $\{w_1\ \ w_2\ldots w_{n_d}\ \ \psi_1\ \ \psi_2\ldots\psi_{n_d}\ \ \theta_1\ \ \theta_2\ldots\theta_{n_j-1}\}^{\mathrm{T}}$, and $n_d$ is the total number of nodes and $n_j$ is the total number of joints in the system.

Similarly, after $i$th locking the torque acting at link $(n-i+1)$ disappears. In addition, $(n-i+1)$th joint loses its rotational degree of freedom and then link $(n-i)$ and $(n-i+1)$ rotate about the $(n-i)$th joint, like a single flexible link $(i+1)$th phase. Thus the two links of length $l_{n-i}$ and $(\sum_{k=1}^{i} l_{n-k+1})$ form a single link of length $(l_{n-i}+\sum_{k=1}^{i} l_{n-k+1})$ and the $(n-i+1)$-link flexible system turns into a $(n-i)$-link flexible system. Thus the equation of the multi-link flexible system after $i$th locking is given by

$$[\mathbf{M}_{i+1}(\mathbf{q}_{i+1})]\{\ddot{\mathbf{q}}_{i+1}\}+[\mathbf{C}_{i+1}(\mathbf{q}_{i+1},\dot{\mathbf{q}}_{i+1})]\{\dot{\mathbf{q}}_{i+1}\}+[\mathbf{K}_{i+1}]\{\mathbf{q}_{i+1}\}=\{\mathbf{W}_{i+1}\}, \tag{21}$$

where $\{\mathbf{q}_{i+1}\}$ is $\{w_1\ \ w_2\ldots w_{n_d}\ \ \psi_1\ \ \psi_2\ldots\psi_{n_d}\ \ \theta_1\ \ \theta_2\ldots\theta_{n_j-i}\}^{\mathrm{T}}$.

Similarly, after $(n-1)$th locking, the second joint loses its rotational degree of freedom and all links rotate about the first joint, like a single flexible link of length $\sum_{k=1}^{n} l_k$ ($n$th phase). In this phase, the equation of motion can be derived as

$$[\mathbf{M}_n(\mathbf{q}_n)]\{\ddot{\mathbf{q}}_n\}+[\mathbf{C}_n(\mathbf{q}_n,\dot{\mathbf{q}}_n)]\{\dot{\mathbf{q}}_n\}+[\mathbf{K}_n]\{\mathbf{q}_n\}=\{\mathbf{W}_n\}, \tag{22}$$

where $\{\mathbf{q}_n\}$ is $\{w_1\ \ w_2\ldots w_{n_d}\ \ \psi_1\ \ \psi_2\ldots\psi_{n_d}\ \ \theta_1\}^{\mathrm{T}}$.

## 3. Numerical results and discussions

In order to demonstrate the performance of the present results, the deployment of a two-link beam structure undergoing locking is compared to those of previous experimental data. Further, the effects of slenderness ratio and shear on the dynamics of a two-link beam structure are investigated, in detail.

### 3.1. Code verifications

In order to verify the present code, an example system of a two-link Timoshenko beam is modeled. Table 1 presents the physical parameters of the system and their actual values, as were used in the experimental setup [5]. Finite element method was used to model the system and a four-node Lagrangian beam element is used.

Fig. 3 presents the resulting angle and angular velocity at each joint for the rigid-body model, flexible model and experimental data [5] during the first phase. The time required for the second joint to reach $0^\circ$ in the flexible system is 2.921 s, slightly longer than that of the rigid-body model (2.895 s) and shorter than that of the experimental data (3.07 s). This is because some part of energy goes into the flexible deformation of the beams in the flexible system. When the angle of the second joint is zero, the angle of the first joint reaches $62.71^\circ$ for the flexible model, $62.69^\circ$ for the rigid-body model and $58.2^\circ$ for the experimental data. The responses of joints for the rigid-body and flexible model are very close because of the small tip displacements of flexible links; however, the response of the angular velocity, of the flexible model shows oscillatory motion about the trajectory of the rigid-body model.

Fig. 4 shows the response of the tip displacement and the velocity of each link in the flexible model during the first phase. The maximum tip displacement of link 1 is 0.696% of $l_1$ and that of link 2 is 0.737% of $l_2$. This is because the rotating velocity of link 2 is faster than that of link 1.

Table 1
System parameters

| | Link 1 | Link 2 |
|---|---|---|
| Length (m) | $l_1 = 1.0064$ | $l_2 = 0.945$ |
| Cross-sectional area ($m^2$) | $A_1 = 1.7808 \times 10^{-4}$ | $A_2 = 1.7748 \times 10^{-4}$ |
| Thickness (m) | $t_1 = 4.4519 \times 10^{-3}$ | $t_2 = 4.4370 \times 10^{-3}$ |
| Area moment of inertia ($m^4$) | $I_1 = 2.9411 \times 10^{-10}$ | $I_2 = 2.9117 \times 10^{-10}$ |
| Rotary inertia ($kgm^2$) | $J_1 = 8.5948 \times 10^{-4}$ | $J_2 = 9.2560 \times 10^{-4}$ |
| Mass density ($kg/m^3$) | $\rho_1 = 2700$ | $\rho_2 = 2700$ |
| Young's modulus ($N/m^2$) | $E_1 = 0.7 \times 10^{11}$ | $E_2 = 0.7 \times 10^{11}$ |
| Tip mass (kg) | $m_{p1} = 1.2$ | $m_{p2} = 0.336$ |
| Torque at joint (Nm) | $\tau_1 = 3.825 \times 10^{-2}$ | $\tau_2 = 0.0225$ |
| Torsion spring stiffness (Nm/rad) | $k_{s1} = 0.0789$ | $k_{s2} = 0.0768$ |
| Pre-rotation angle (deg) | $\theta_{01} = 300$ | $\theta_{02} = 60$ |

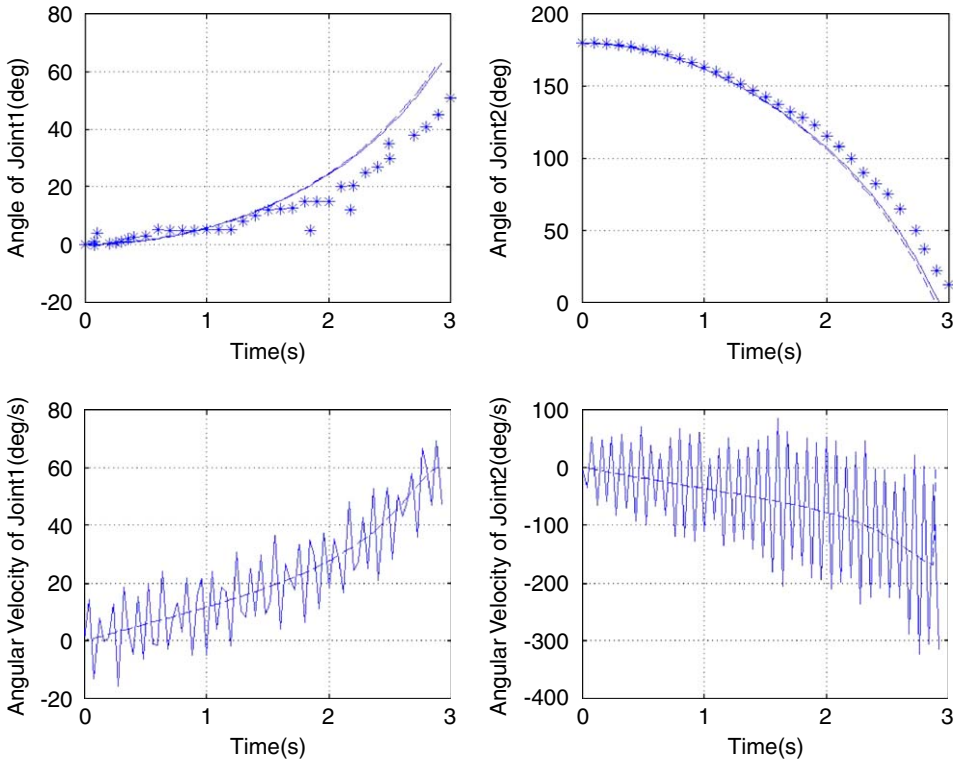


Fig. 3. Angle and angular velocity of each joint during the first phase; — flexible model, - - rigid-body model, * experimental data [5].

Fig. 5 describes the angle and angular velocity of joint 1 during the second phase. There is a significant difference in the responses for these two parameters between the flexible and rigid-body model during the second phase. Angle of joint 1 in the rigid-body model increases linearly after locking while that in the flexible model, oscillates and increases only slightly similar to that of the experimental data. However, there is a little difference between the results of the flexible model and experimental data after locking, the joint 1 angle of the experimental data oscillates at a higher amplitude compared to that of the flexible model. This may be due to the structural damping of arms, the backlash effects, friction and other disturbances in the experimental model which were not modeled in the numerical simulations.

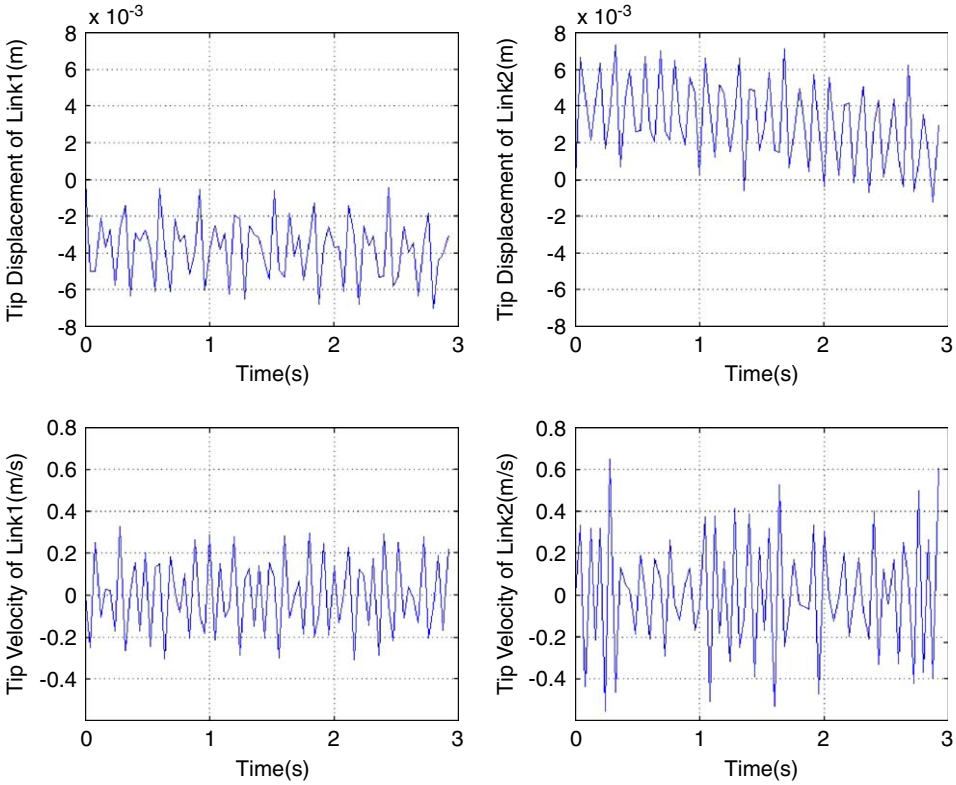


Fig. 4. Tip displacement and the velocity of each link during the first phase.

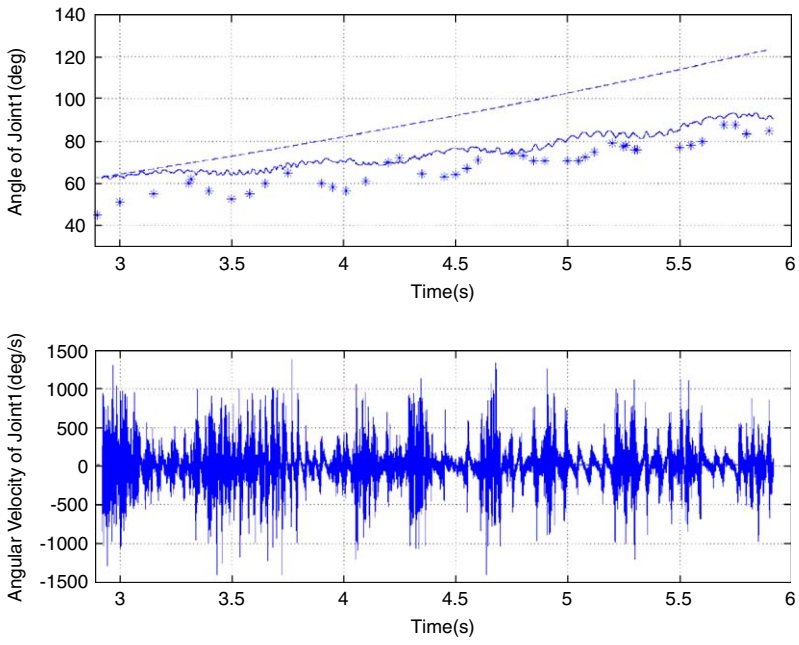


Fig. 5. Angle and angular velocity of joint 1 during the second phase; — flexible model, - - rigid-body model, * experimental data [5].

The tip displacement and velocity of each link in the flexible model during the second phase are represented in Figs. 6 and 7. The tip displacement of the second phase is larger than that of the first phase. The maximum tip displacement of links 1 and 2 are 2.455% and 8.012% of total length ($l_1 + l_2$), respectively. When the second joint locks in the flexible model, some of link 2's kinetic energy is transformed into elastic and kinetic energy, which increase tip displacement and velocity after locking. Thus the joint of a single flexible link oscillates during motion.

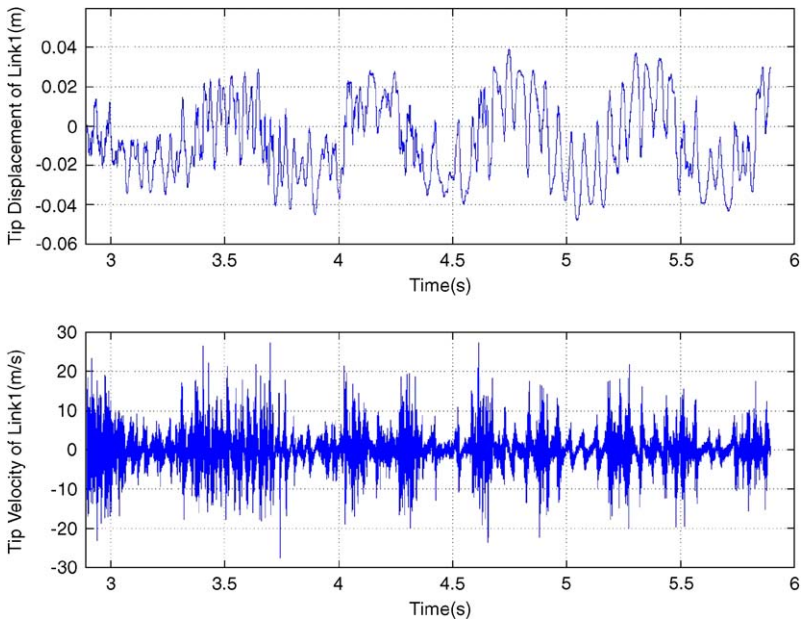


Fig. 6. Tip displacement and the velocity of link 1 during the second phase.

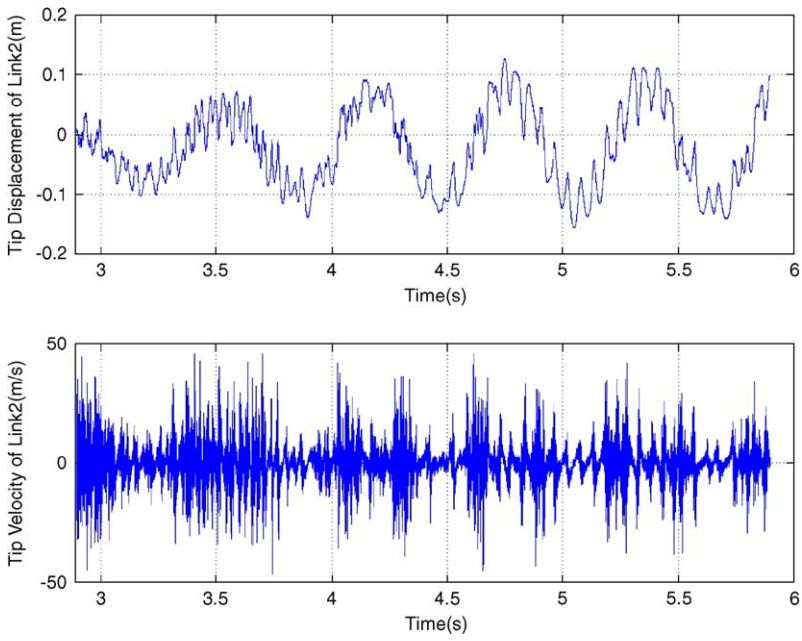


Fig. 7. Tip displacement and the velocity of link 2 during the second phase.

### 3.2. Effect of slenderness ratio

To analyze the effect of thickness on the dynamics of a two-link beam structure, the angle and tip displacement of each link are compared as the slenderness ratio ($t/l$) is varied. The length and the cross-sectional area of each link are assumed to be constant. Thus the mass of the structure is not changed according to the various slenderness ratios. The slenderness ratios used in code verifications are 0.0044 for link 1 and 0.0047 for link 2.

Fig. 8 shows the angle of each joint during the first phase as the slenderness ratios are increased by 1, 2, 5 and 10 times. This shows that the varied slenderness ratios have almost no effect on the angle of each joint and locking time. The code verification produced similar result, in that, the angle of each joint in the flexible model is very close to that of the rigid-body model during the first phase. Thus, before locking, it is observed that the angle of each joint and locking time for varied slenderness ratio are hardly changed when the mass of the structure is assumed to be constant.

Fig. 9 shows the tip displacement of each link as the slenderness ratio is varied during the first phase. In this, S.R. denotes the slenderness ratio of each beam for a two-link beam structure. When the slenderness ratio is increased, the tip displacement of each link decreases, and amplitude decreases and frequency increases. When the slenderness ratio is 10 times the input data, the tip displacement of each link approaches zero and the motion of flexible system becomes similar to that of rigid-body model. This is because as the slenderness ratio is increased, the beam becomes stiffer and tends towards rigid. As a result, the slenderness ratio is a very important factor for displacement before locking.

Fig. 10 describes the angle of joint 1 as the slenderness ratio is varied during the second phase. When the slenderness ratio is increased, the amplitude decreases and the frequency increases. When the slenderness ratio is increased 2–5 times, the angle of joint 1 decreases; however, when the slenderness ratio is increased 10 times, the angle of joint 1 becomes larger than that of when the slenderness ratio was increased five times but smaller than that of when the slenderness ratio was increased two times. This shows the convergence of the angle for joint 1 to that of rigid-body model.

The results show that the slenderness ratio does not affect the system motion significantly with no locking but does so significantly if there is locking. Therefore, the slenderness ratio has almost no effect on pre-lock deployment, however becomes a very important factor of post-lock deployment.

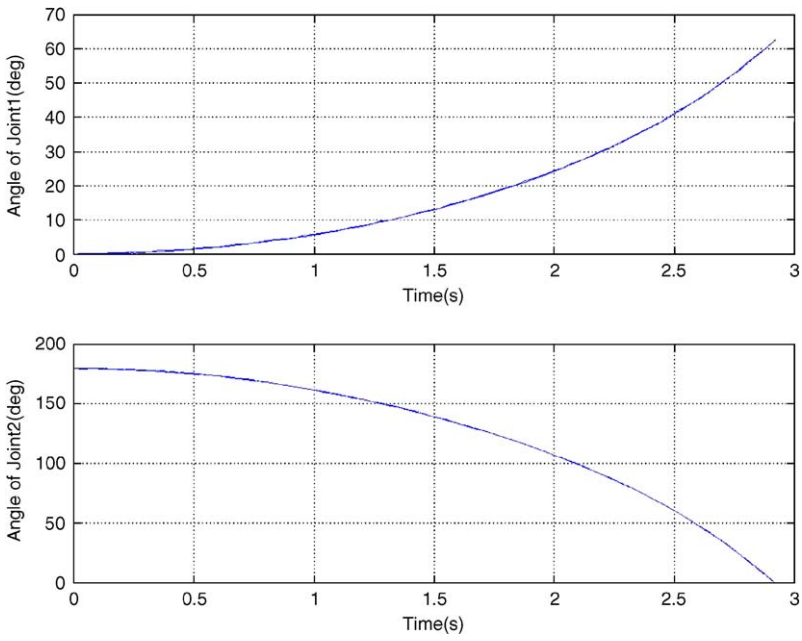


Fig. 8. Angle of joints during the first phase at various slenderness ratio.

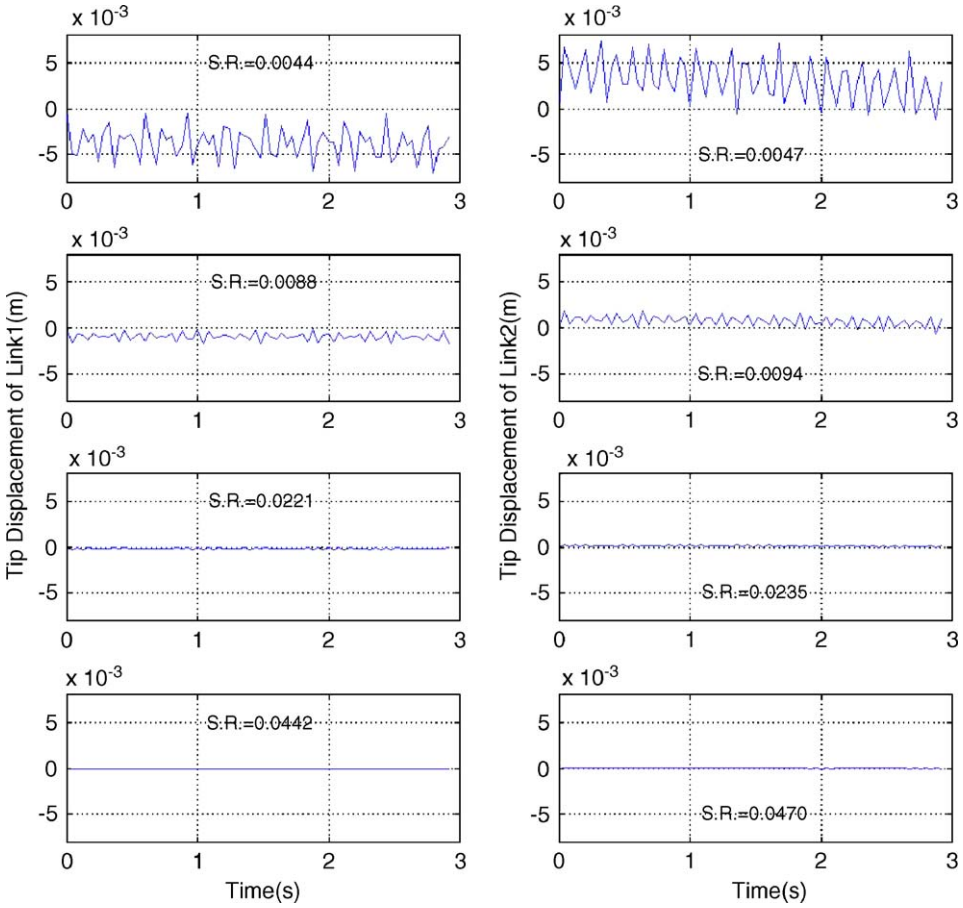


Fig. 9. Tip displacement of each link during the first phase according to slenderness ratio.

The tip displacement of each link according to the slenderness ratio during the second phase is shown in Fig. 11. In this figure, S.R. indicates the slenderness ratio of a single link beam. Like the responses during the first phase, the tip displacement of each link decreases, and the amplitude decreases and the frequency increases as the slenderness ratio is increased. When the slenderness ratio is 10 times the input data, the tip displacement of each link approaches zero and the motion of flexible system becomes similar to that of rigid-body model.

Thus, the slenderness ratio is a very important factor of pre- and post-lock displacement.

### 3.3. *Effect of shear*

In order to investigate the effect of shear, the tip displacements of a two-link Timoshenko beam are compared with those of a two-link Euler–Bernoulli beam when the slenderness ratios are two times the input data.

Fig. 12 describes the tip displacement of each link during the first phase. This shows that the response of an Euler–Bernoulli beam is very similar to that of a Timoshenko beam. Thus, the shear has almost no effect on the deployment of the structure before locking.

The tip displacements of link 1, 2 during the second phase are depicted in Fig. 13. The response during the second phase is very different comparing to that during the first phase. It is found that the effect of shear is considerable during the second phase. The tip displacement of each link for an Euler–Bernoulli beam is larger

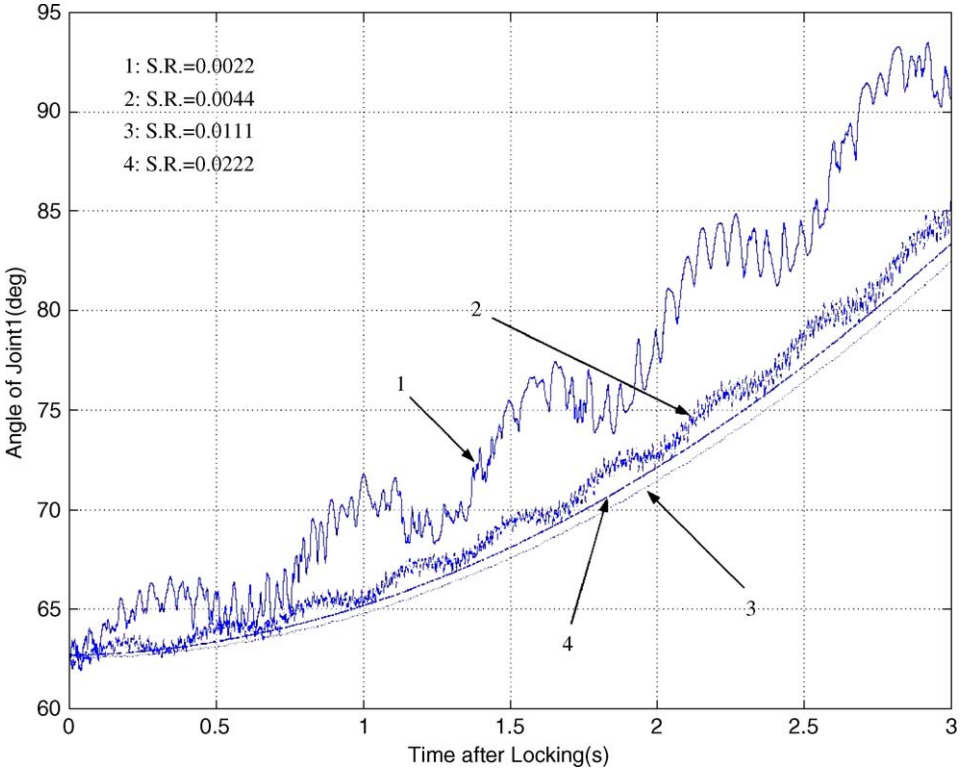


Fig. 10. Angle of joint 1 during the second phase according to slenderness ratio.

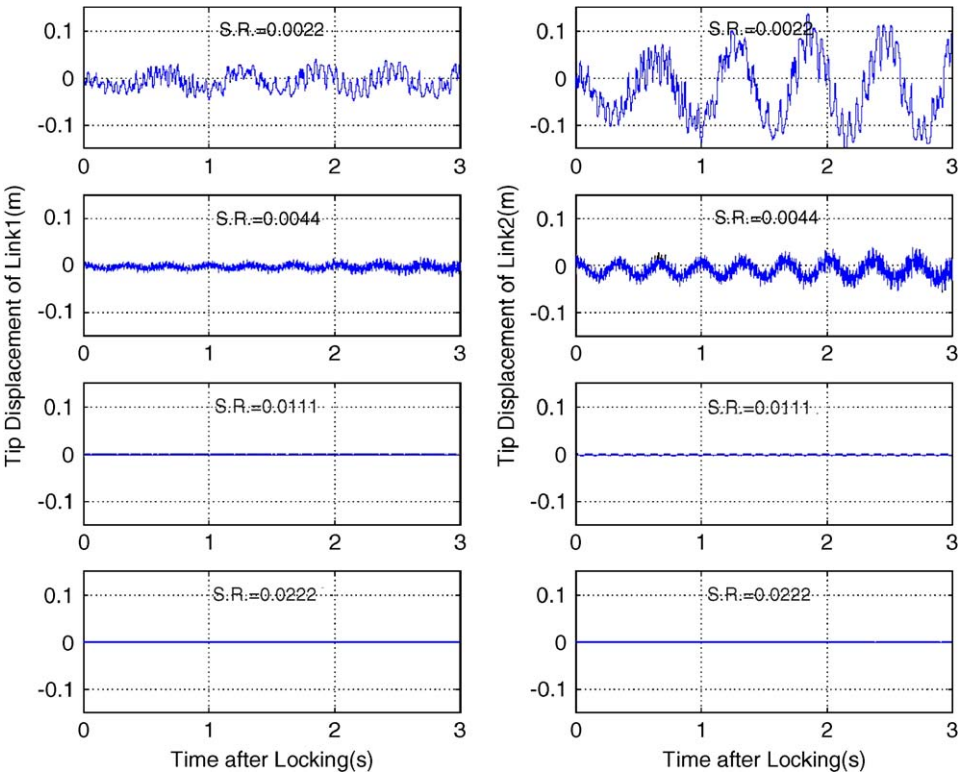


Fig. 11. Tip displacement of each link during the second phase according to slenderness ratio.

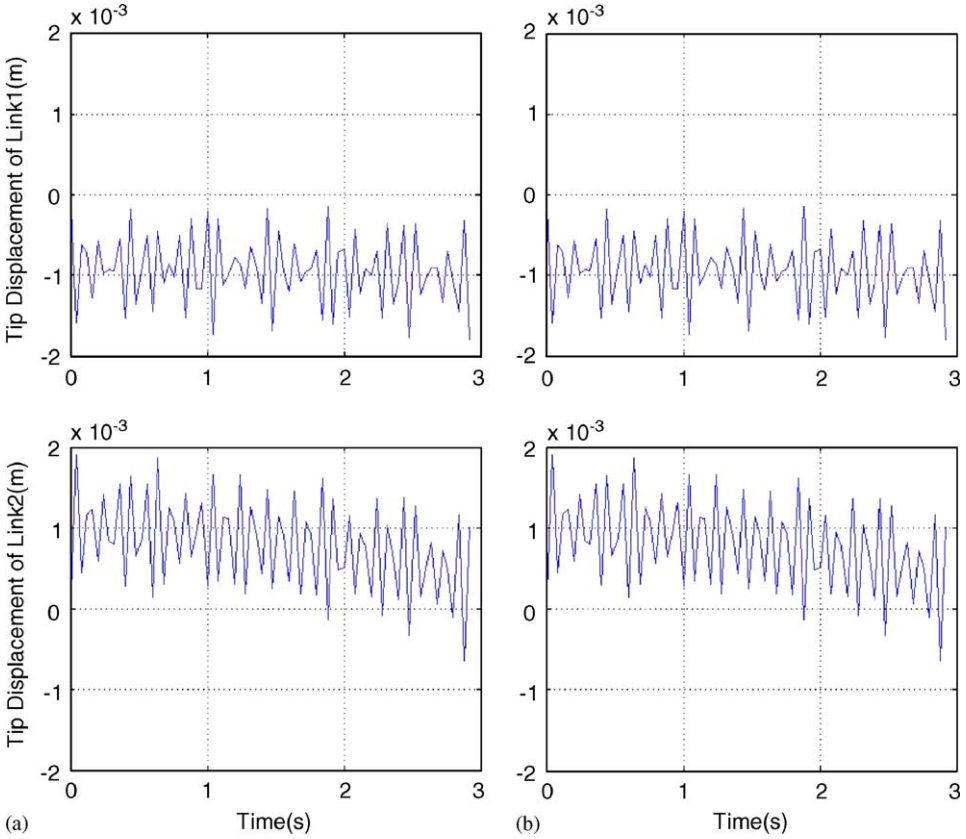


Fig. 12. Tip displacement of each link during the first phase: (a) two-link Timoshenko beam; (b) two-link Euler–Bernoulli beam.

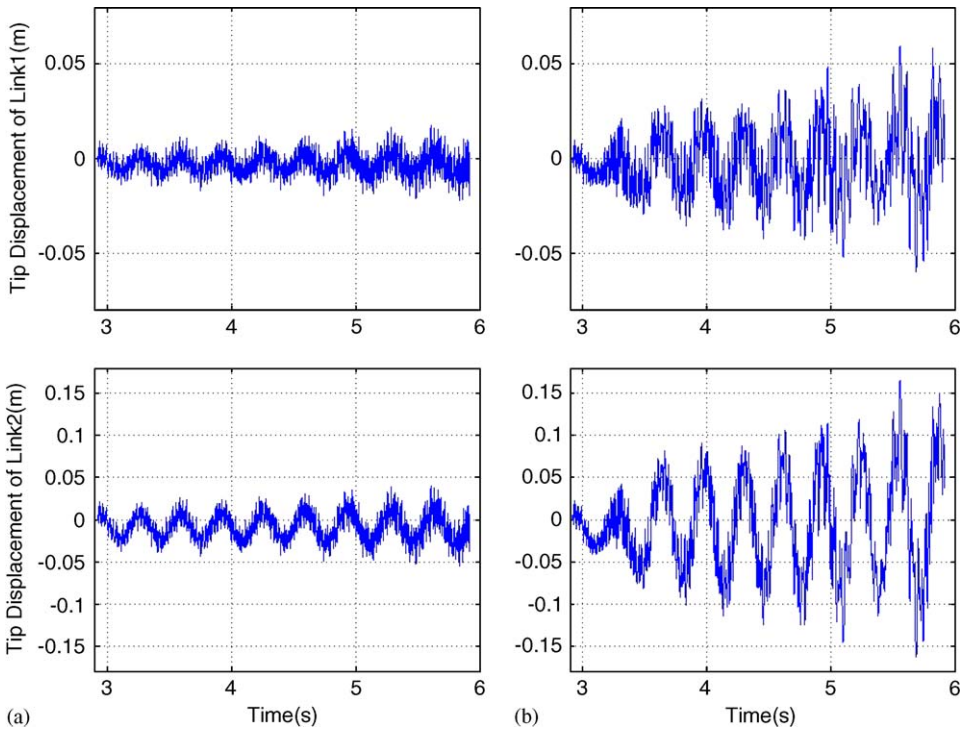


Fig. 13. Tip displacement of each link during the second phase: (a) two-link Timoshenko beam; (b) two-link Euler–Bernoulli beam.

than that for a Timoshenko beam conspicuously. However, the frequencies of the tip displacements for an Euler–Bernoulli beam are similar to those for a Timoshenko beam.

As a result, shear has great effect on the deployment of the structure which undergoes locking.

## 4. Conclusions

The deployment of a multi-link beam structure which undergoes locking is compared to that of the previous work and the effects of slenderness ratio and shear are investigated.

The responses of the model for Timoshenko beam follow the experimental data more approximately than those of the rigid-body model. There is only a slight difference in the responses between the flexible and rigid-body model during the first phase, but difference becomes more significant after locking. This shows that the deployment of a multi-link system undergoing locking must be analyzed as a flexible system.

In order to investigate the effect of thickness in the dynamics of a two-link beam structure, the angle and tip displacement of each link is compared as the slenderness ratio is varied. The length and the cross-sectional area of each link are assumed to be constant. As a result, during the first phase the slenderness ratios have almost no effect on the angle of each joint and locking time. On the other hand, the slenderness ratios affected the tip displacement of each link considerably. As the slenderness ratio is increased, the tip displacement and the amplitude of each link decrease, however, the frequency increases. During the second phase, as the slenderness ratio is increased, the amplitude of the angle for joint 1 decreases and the frequency increases. The tip displacement of each link during the second phase is similar to that of the first phase. This shows that the responses after locking change greatly according to the slenderness ratio. In view of the results so far achieved, the slenderness ratio has great effect on the deployment after locking, and also on the displacement of each link before and after locking.

To analyze the effect of shear, the tip displacements of a two-link Timoshenko beam are compared to those of a two-link Euler–Bernoulli beam. The shear has almost no effect on the tip displacements of the structure before locking. However, it has great effect on the tip displacements of the structure after locking. The tip displacement of each link for an Euler–Bernoulli beam is larger than that for a Timoshenko beam conspicuously, after locking. As a result, shear has great effect on the deployment of the system which undergoes locking.

## Acknowledgments

This work was supported by the Brain Korea 21 project.

## References

[1] L. Meirovitch, Y. Chen, Trajectory and control optimization for flexible space robots, *Journal of Guidance, Control, and Dynamics* 18 (1995) 493–502.

[2] A.S. Yigit, The effect of flexibility on the impact response of a two-link rigid-flexible manipulator, *Journal of Sound and Vibration* 177 (1994) 349–361.

[3] S. Yu, M.A. Elbestawi, Modelling and dynamic analysis of a two-link manipulator with both joint and link flexibilities, *Journal of Sound and Vibration* 179 (1995) 839–854.

[4] S.S. Ge, T.H. Lee, G. Zhu, Non-model-based position control of a planar multi-link flexible robot, *Mechanical Systems and Signal Processing* 11 (1997) 707–724.

[5] B.P. Nagaraj, B.S. Nataraju, Dynamics of a two-link flexible system undergoing locking: mathematical modelling and comparison with experiments, *Journal of Sound and Vibration* 207 (1997) 567–589.

[6] R.F. Fung, H.C. Chang, Dynamic modelling of a non-linearly constrained flexible manipulator with a tip mass by Hamilton's principle, *Journal of Sound and Vibration* 216 (1998) 751–769.

[7] R.I. Milford, S.F. Asokanthan, Configuration dependent eigenfrequencies for a two-link flexible manipulator: experimental verification, *Journal of Sound and Vibration* 222 (1999) 191–207.

[8] W. Chen, Dynamic modeling of multi-link flexible robotic manipulators, *Computers and Structures* 79 (2001) 183–195.

[9] S. Hariharesan, A.A. Barhorst, Modelling, simulation and experimental verification of contact/impact dynamics in flexible multi-body systems, *Journal of Sound and Vibration* 221 (1999) 709–732.

[10] J.L. Escalona, J.M. Mayo, J. Dominguez, A critical study of the use of the generalized impulse-momentum balance equations in flexible multibody systems, *Journal of Sound and Vibration* 217 (1998) 523–545.
[11] M. Farid, S.A. Lukasiewicz, Dynamic modeling of spatial manipulators with flexible links and joints, *Computers and Structures* 75 (2000) 419–437.
[12] G. Naganathan, A.H. Soni, Coupling effects of kinematics and flexibility in manipulators, *The International Journal of Robotics Research* 6 (1987) 75–84.
[13] M. Iura, S.N. Atluri, Dynamic analysis of planar flexible beams with finite rotations by using inertial and rotating frames, *Computers and Structures* 55 (1995) 453–462.
[14] J. Cheong, Y. Youm, W.K. Chung, Accessibility and identifiability of horizontal vibration in 3-D two-link flexible robots: system mode approach, *Journal of Sound and Vibration* 269 (2004) 489–509.
[15] R.J. Theodore, A. Ghosal, Robust control of multilink flexible manipulators, *Mechanism and Machine Theory* 38 (2003) 367–377.
[16] K.J. Bathe, *Finite Element Procedures*, Prentice-Hall, New Jersey, 1996.
[17] D.T. Greenwood, *Classical Dynamics*, Prentice-Hall, New Jersey, 1977.